CRYSTAL GROWTH & DESIGN

pubs.acs.org/crystal

Article

$Ce_4B_2C_2F_{0.14}H_{2.26}$: Cerium Borocarbides with Fluoride and Hydride Interstitials Grown from Ce/Cu Flux

James T. Larson, Christina Hoffmann, and Susan E. Latturner*

Cite This: *Cryst. Growth Des.* 2023, 23, 5919−5924

Read Online

ACCESS | Metrics & More | Article Recommendations | Supporting Information

ABSTRACT: Fluoride interstitials were introduced into an intermetallic structure by carrying out metal flux growth in the presence of a fluorocarbon. Decafluorobiphenyl and anthracene were reacted with boron in a melt composed of cerium and copper, yielding crystals of $Ce_4B_2C_2F_{0.14}H_{2.26}$, a fluorinated analogue of previously reported $Ce_4B_2C_2H_{2.42}$. The siting and occupancies of the fluoride and hydride interstitials were confirmed using both single-crystal X-ray diffraction and neutron diffraction. The fluoride mixes with the hydride in an octahedral interstitial site surrounded by cerium cations; additional hydride ions occupy the tetrahedral sites. Magnetic susceptibility shows a change from canted antiferromagnetic ordering reported for the hydride to paramagnetic behavior upon fluorine substitution.

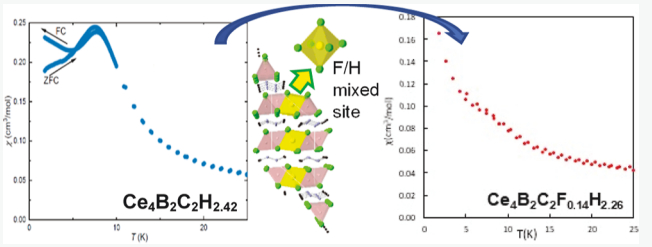

INTRODUCTION

Rare-earth intermetallics are of interest due to their complex and potentially useful magnetic properties. Magnetic interactions between rare-earth ions are mediated by RKKY coupling, which is distance dependent.[1,2] Modifying the distance between the ions can lead to a change in the magnetic coupling forces and ordering temperature. One method of controlling R−R distances is to introduce interstitial elements into the structure. This typically expands the unit cell, increasing the R−R distance. Interstitial chemistry of cerium intermetallics offers a particularly rich arena to explore. In addition to long-range magnetic ordering, cerium can have unusual magnetic properties due to its ability to be in the trivalent state or the tetravalent state. This can lead to Kondo lattice physics and heavy fermion behavior. Introducing interstitials may be a way to tailor these complex behaviors.

Rare-earth-rich intermetallic phases can be grown as well-formed crystals from metal flux reactions in eutectic melts composed of a rare-earth and a transition metal. For instance, the Ce/Cu eutectic (72 mol % Ce) melts at 424 °C, and the Ce/Ni eutectic (82 mol % Ce) melts at 532 °C.[3,4] Reactions in these eutectic fluxes have produced a variety of cerium intermetallics such as $Ce_{21}Fe_8Bi_7C_{12}$, $Ce_{10}Co_{2.46}B_{11.70}C_{10}$, and $Ce_{33}Fe_{13.1}Al_{1.1}B_{24.8}C_{34}$.[5−7] Recently, we have found that using a hydrocarbon such as anthracene as a reactant can introduce hydride interstitials into products. The presence of hydrides in $La_{15}(FeC_6)_4H$, $Ce_4B_2C_2H_{2.42}$, and $La_3BC_2H_{1.69}$ was confirmed by neutron diffraction. These species are located in either tetrahedral or octahedral interstitial sites surrounded by rare-earth cations.[8,9]

We are now exploring the use of fluorocarbon reactants to introduce fluoride interstitials which are easier to detect via SCXRD. In this work, we reacted decafluorobiphenyl ($C_{12}F_{10}$) and anthracene ($C_{14}H_{10}$) with boron and carbon in a cerium/copper eutectic. This produced the title compound $Ce_4B_2C_2F_{0.14}H_{2.26}$, which formed as sufficiently large crystals for neutron diffraction. Single-crystal neutron diffraction data indicated the presence of hydride in the tetrahedral interstitial sites and a mixture of hydride and fluoride in the octahedral interstitial sites. Density of state (DOS) calculations and magnetic susceptibility measurements were performed to compare the properties of the fluorinated compound to the hydrogen analogue $Ce_4B_2C_2H_{2.42}$.

EXPERIMENTAL PROCEDURE

Synthesis. The Ce/Cu flux was made with a ratio of 74:26 mol %. This ratio is slightly higher in cerium than the actual Ce/Cu eutectic point of 72:28 mol % to account for the loss of cerium from solution as it is incorporated into the product; the presence of excess Ce ensures that the Ce/Cu flux mixture will remain near the low-melting eutectic point. Cerium ingots (99.9% Strem Chemicals) and copper slugs (99.995% Alfa Aesar) were arc-melted under argon, and the resulting pellet was flipped and remelted several times to ensure complete mixing. This pellet was then broken into pieces using metal snips for use as a flux. Initial reactions of decafluorobiphenyl ($C_{12}F_{10}$, TCI 98.0%), boron powder (Alfa Aesar 98% metal basis), and the Ce/Cu flux were carried out in alumina crucibles using a reactant ratio of 0.1 mmol of $C_{12}F_{10}$, 1 mmol of B, and 1.5 g of flux. It was found that $C_{12}F_{10}$ needed to be placed outside the crucible itself to avoid initial fluorination side reactions. Therefore, boron was loaded into

Received: April 26, 2023
Revised: June 21, 2023
Published: July 6, 2023

the crucible first and the pieces of Ce/Cu flux on top of that. The $C_{12}F_{10}$ powder was placed into the silica sleeve just below the alumina crucible (see Figure S1, Supporting Information). A wad of Fiberfrax was placed above the alumina crucible to act as a filter. The silica sleeve was cooled in an ice bath (to lower the volatility of the organic reactants) while being evacuated to 100 mTorr; it was then flame-sealed under vacuum and placed in a programmable furnace. The reaction was heated to 1000 °C in 3 h, held at 1000 °C for 6 h, cooled to 850 °C over the course of 24 h, held there for 18 h, and gradually cooled to 550 °C in 96 h at which point it was taken out of the furnace and the flux was centrifuged off.

The above reaction produces a low yield of the title compound as very small crystals, with a large amount of powder byproduct. This reaction could not be reproduced reliably, indicating that the desired product was resulting from incorporation of a contaminant, possibly hydride from surface hydroxides. Therefore, a hydride source (anthracene) was deliberately added. Anthracene ($C_{14}H_{10}$, Sigma-Aldrich, 97%) and boron powder were weighed out with ratios of 0.03:1 mmol and placed in an alumina crucible in that order, with 1.5 g of Ce/Cu flux placed on top. 0.05 mmol of decafluorobiphenyl was placed inside of the silica sleeve at which point the alumina crucible containing the rest of the reactants was placed on top (see the Supporting Information). The silica ampule was flame-sealed, and the reaction was heated and then centrifuged as described above. With the introduction of a hydride source, the reaction became reproducible, indicating that the product likely contains both fluoride and hydride.

Elemental Analysis. Elemental analysis was done using a FEI NOVA 400 scanning electron microscope equipped with energy-dispersive X-ray spectroscopy (SEM–EDS). The crystals of the $Ce_4B_2C_2F_{0.14}H_{2.26}$ product were mounted on an aluminum puck using double-sided carbon tape. To eliminate spurious readings from the flux residue on the surface, each crystal was cleaved and arranged on the carbon tape so that an inside surface was perpendicular to the electron beam. An acceleration voltage of 30 kV was used for EDS measurements. EDS confirmed the presence of cerium and fluorine as well as boron and carbon; however, the amount of boron and carbon cannot be quantitatively determined due to the limitations of the EDS detector toward light elements and the background due to use of carbon tape. Removing these light elements from the quantification yields Ce and F atomic percentages of 82(2) and 18(2)%, respectively. This corresponds to a ratio of $Ce_4B_2C_2F_{0.88}$. This is richer in fluorine than indicated by diffraction studies (vide infra), possibly due to the light element being at the threshold of EDS quantitative analysis. Incorporation of copper from the flux was not observed. Elemental mapping scans (Figure 1) show uniform distribution of cerium and fluorine through the cleaved crystal.

Structural Characterization—X-ray Diffraction. Single-crystal samples were selected that were clean of surface flux and mounted onto cryoloops with Parabar oil. This oil holds the crystals in place on the loop without contributing to the diffraction signal. Single-crystal X-ray diffraction (SC-XRD) data were collected at 100 K on a Rigaku XtaLAB Synergy-S diffractometer equipped with a HyPix-6000HE Hybrid Photon Counting (HPC) detector and Mo/Cu microfocus sealed X-ray sources. The CrysalisPRO software was used to integrate the raw data, and the structures were then imported into the Shelxle program suite and the structure solved using direct methods in order to locate cerium atoms, while positions of boron and carbon were found through the combined use of least-squares refinement and difference Fourier maps.[10,11] An electron density peak corresponding to the octahedral interstitial was also apparent in the difference map, and this was assigned as fluorine. However, given that this is a light atom on a high-symmetry special position (which is prone to ghost peaks), neutron diffraction data were also collected. The thermal parameters of cerium and boron were refined anisotropically; those of carbon and fluorine were refined isotropically with the latter constrained to be similar to those of boron and carbon.

Structural Characterization—Neutron Diffraction. Single-crystal neutron diffraction data were collected using the TOPAZ diffractometer (BL-12, SNS) at Oak Ridge National Laboratory. A single crystal (dimensions 1.55 mm × 0.50 mm × 0.45 mm) was

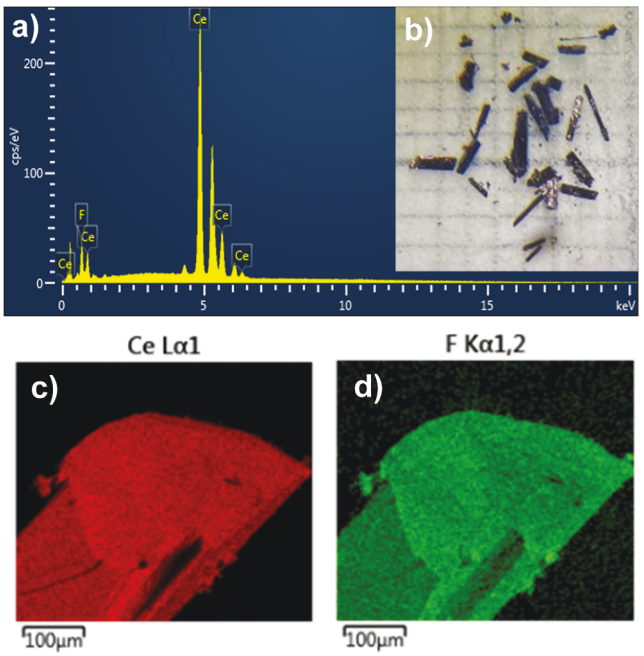

Figure 1. (a) EDS spectra of $Ce_4B_2C_2F_{0.14}H_{2.26}$. (b) Optical microscopic image on millimeter grid paper. (c) EDS elemental mapping image for cerium. (d) EDS elemental mapping image for fluorine.

mounted onto a 1 mm MiTiGen tip and held in place with Krytox grease. Data were collected at 100 K using 20 crystal orientations determined using the CrystalPlan software which calculated optimal coverage for the monoclinic I setting of the unit cell.[12] To account for normal fluctuations in the output power of the neutron beam, each orientation was exposed to the neutron beam until it had collected 15C of charge, which required about 3–4 h of exposure at a nominal neutron beam power of 1.4 MW. Integrated peak intensities were analyzed using the Mantid platform.[13] Data reduction was carried out using the ANVRED3 program (including neutron TOF spectra, detector efficiency, and absorption corrections).[14] Face indexing was carried out to correct for absorption anisotropy. The cell was transformed to the conventional monoclinic C setting for final refinement cycles. Crystallographic data and collection parameters are shown in Table 1; additional information is deposited in the Cambridge Crystallographic Data Centre with deposition numbers CSD-2259229 (X-ray data) and CSD-2259230 (neutron data).

Magnetic Susceptibility Measurements. Magnetic susceptibility measurements were performed on the title compound to compare its behavior to that of the isostructural hydride $Ce_4B_2C_2H_{2.42}$ reported by Hertz et al.[9] Multiple single crystals were placed on a piece of Kapton tape with their *b*-axes aligned parallel to the magnetic field. The Kapton tape was then wrapped around a straw and attached to the end of the sample rod. Magnetic susceptibility $\chi = M/H$ data were collected from 1.8 to 300 K under an applied magnetic field of H = 2000 Oe using a Quantum Design MPMS SQUID system. Magnetization measurements were collected at 1.8 K, with the applied field from $-7\ T < H < 7\ T$.

Electronic Structure Calculations. The Stuttgart TB-LMTO-ASA (tight binding linear muffin tin orbital atomic sphere approximation) program package was used to calculate the DOS.[15] Calculations were performed on two models which differed in interstitial content; both models were derived from unit cell parameters and atomic coordinates determined by the single-crystal neutron structure of $Ce_4B_2C_2F_{0.14}H_{2.26}$ at 100 K. Cerium is modeled as lanthanum to avoid computational issues that stem from partially filled f-shells. In the first model ($La_4B_2C_2FH_2$), the octahedral mixed site is filled with fluorine and the tetrahedral hydrogen site is modeled as fully occupied. In the second model ($La_4B_2C_2H_3$), the octahedral

https://doi.org/10.1021/acs.cgd.3c00512
Cryst. Growth Des. 2023, 23, 5919–5924

Table 1. Crystallographic Data and Collection Parameters for $Ce_4B_2C_2F_{0.14}H_{2.26}$

	XRD	neutron diffraction
formula weight (g/mol)	610.98	
crystal system	monoclinic	
space group	$C2/m$ (no. 12)	
a (Å)	12.792(3)	12.6978(2)
b (Å)	3.7475(3)	3.7566(4)
c (Å)	9.4782(2)	9.7155(1)
β (deg)	130.65(3)	132.297(8)
Z	2	
volume (Å^3)	344.76(2)	342.79(5)
density, calc (g/cm^3)	5.865	5.919
index ranges	$-15 \le h \le 14$	$-22 \le h \le 22$
	$-5 \le k \le 5$	$-6 \le k \le 6$
	$-12 \le l \le 13$	$-17 \le l \le 17$
reflections collected	2201	4588
temperature (K)	100	97
radiation	Mo Kα (λ = 0.71073 Å)	neutron TOF
unique data/parameters	487/24	1121/38
reflections theta max	30.889	77.633
μ (mm^{-1})	25.783	0.0200 + 0.4957λ
R_1/wR_2	0.0409/0.0984	0.0715/0.1484
R_1/wR_2 (all data)	0.0463/0.1071	0.0763/0.1503
GoF	1.111	1.364
highest peak/hole (e$^-$/Å^3)	2.524/−3.389	1.359/−1.360

mixed site is filled with hydrogen, and the tetrahedral hydride site is fully occupied. The following basis sets were used: La (6s, 5d, and 4f), C (2s and 2p), B (2s and 2p), F (2s and 2p), and H(1s), with La (6p), C (3d), F (3d), and B (3d) being downfolded. Integration over the Brillouin zone was made by the tetrahedron method.[16]

RESULTS AND DISCUSSION

Our previous work using anthracene as both a carbon and a hydrogen source during metal flux synthesis has yielded several new compounds containing hydride interstitials, including $La_{15}(FeC_6)_4H$ and $Ce_4B_2C_2H_{2.42}$.[8,9] During the flux reaction, the thermal decomposition of the anthracene yields carbon (some of which is deposited on the walls of the silica ampule) and hydrogen gases, which incorporates into products growing in the flux. We are now exploring the use of fluorocarbons to see if fluorine interstitials can be incorporated into flux-grown intermetallic compounds. Unlike hydride, fluoride has sufficient electron density to be detected using standard SC-XRD measurements. A major obstacle is the high electronegativity of fluorine and the stability of ionic metal fluorides, which are thermodynamically preferred compared to formation of an intermetallic with fluoride interstitials.[17] Given the successful reactions using anthracene (an easily weighable, air-stable, high melting aromatic hydrocarbon), decafluorobiphenyl ($C_{12}F_{10}$) was chosen as the fluorine source. This method was recently found to be successful in the formation of $La_{15}(FeC_6)_4F_2$, which was grown from the reaction of iron and $C_{12}F_{10}$ in La/Ni flux.[18] This is a fluorinated analogue of $La_{15}(FeC_6)_4H$ (formed from reaction of iron and $C_{14}H_{10}$ in La/Ni flux).[8] Further support for decomposition of a fluorocarbon as a source of fluorine is found in a recent report involving post-synthesis topotactic fluorination of the intermetallic LaFeSi. This compound was exposed to a flow of C_4F_8 at elevated temperature, and fluorine was found to incorporate onto tetrahedral interstitial sites, forming $LaFeSiF_x$.[17]

Synthesis. In the method explored here, the thermal degradation of fluorocarbons and hydrocarbons occurs as the flux reaction is heating, and the degradation products (carbon, F_2, and H_2) are incorporated into the melt to act as reactants. Initial reactions using only $C_{12}F_{10}$ produced a low yield, indicating that the desired product was resulting from incorporation of a required element initially present as a contaminant, possibly hydride from surface hydroxides. Therefore, a hydride source (anthracene) was deliberately added. It was found that a too high amount of anthracene will change the boron/carbon ratio, leading to a competing phase (orthorhombic $Ce_3BC_2H_x$, manuscript in progress).

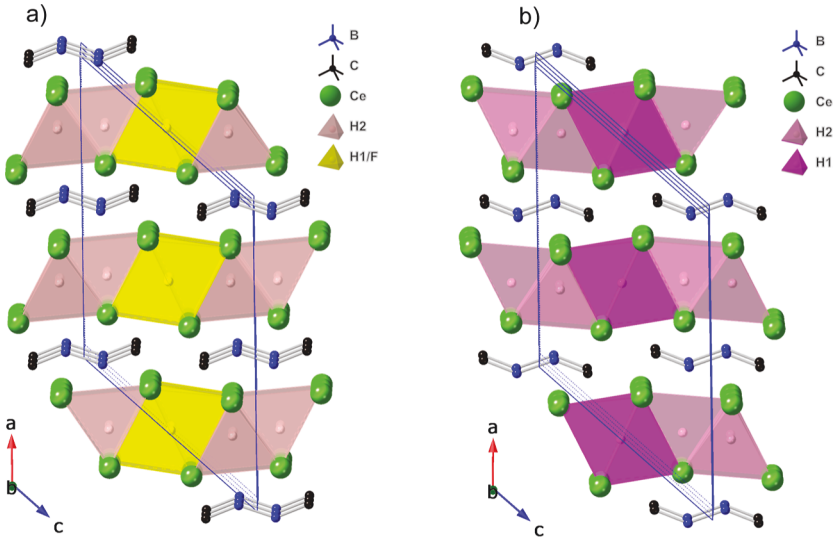

Figure 2. Structures of $Ce_4B_2C_2F_{0.14}H_{2.26}$ (left) and $Ce_4B_2C_2H_{2.42}$ (right) shown in the polyhedral mode viewed down the b-axis. (a) $Ce_4B_2C_2F_{0.14}H_{2.26}$; yellow polyhedra are the mixed F/H octahedral site with a F occupancy of 14(2) % and a H occupancy of 84(5) %. Pink polyhedra are tetrahedral hydride sites with an occupancy of 71(2) %. (b) $Ce_4B_2C_2H_{2.42}$; purple polyhedra are hydride octahedral sites with an occupancy of 42%, and pink polyhedra are fully occupied tetrahedral hydride sites.

https://doi.org/10.1021/acs.cgd.3c00512
Cryst. Growth Des. 2023, 23, 5919−5924

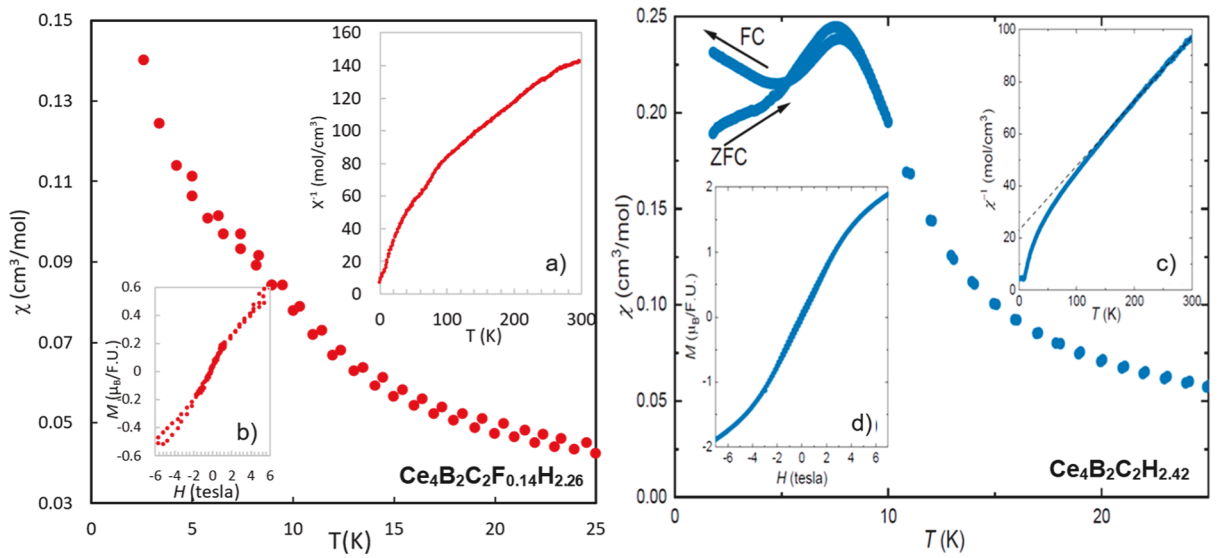

Figure 3. Comparison of magnetic susceptibility temperature dependence data of $Ce_4B_2C_2F_{0.14}H_{2.26}$ (left, data in red) with $Ce_4B_2C_2H_{2.42}$ (right, data in blue), both collected with an applied external field of 0.2 tesla. Insets (a) and (c) are inverse susceptibility data $1/\chi$ vs T; insets (b) and (d) are field-dependent magnetization data collected at 1.8 K.

The optimal reactant ratio that enables the formation of crystals of the title phase is the reaction of 1 mmol of B, 0.028 mmol of $C_{14}H_{10}$, and 0.05 mmol of $C_{12}F_{10}$ in 1.5 g of Ce/Cu flux. The yield is highly dependent on the amount of decafluorobiphenyl. If less than 0.03 mmol of $C_{12}F_{10}$ is used, the reaction produces the previously reported hydride analogue, $Ce_4B_2C_2H_{2.4}$. If more than 0.07 mmol of $C_{12}F_{10}$ is used, the product is a powdered mixture including boron, metal fluorides, and other compounds. $Ce_4B_2C_2F_{0.14}H_{2.26}$ crystals are dark silver rods up to 3 mm long, with an average of approximately 1.5 mm in length; the width ranges from 0.1 to 0.3 mm. This compound decomposes when exposed to air, but it can be briefly handled in air to mount crystals under Parabar oil.

Structure. $Ce_4B_2C_2F_{0.14}H_{2.26}$ crystallizes in the monoclinic space group $C2/m$; the structure is shown in Figure 2. Like the previously reported hydride $Ce_4B_2C_2H_{2.42}$, the title compound is a stuffed variant of Nd_2BC, with light atoms in the octahedral and tetrahedral interstitial sites defined by rare-earth atom positions. These rare-earth layers are separated by layers of borocarbide chains. Comparing the unit cell parameters of $Ce_4B_2C_2F_{0.14}H_{2.26}$ to those of $Ce_4B_2C_2H_{2.42}$, the fluoride has a smaller a-axis and slightly larger b- and c-axes, leading to an overall decrease of the cell volume from 350.9(1) Å^3 for $Ce_4B_2C_2H_{2.42}$ to 342.79(5) Å^3 for $Ce_4B_2C_2F_{0.14}H_{2.26}$.

The positions of boron and carbon atoms in $Ce_4B_2C_2F_{0.14}H_{2.26}$ were determined by comparing the bond lengths. The B−C bond length in the [C−B−B−C] unit is 1.499(5) Å, and the B−B distance is 1.648(8) Å. This is comparable with the B−C distance of 1.506(1) Å and the B−B distance of 1.660(2) Å observed for the same unit in $Ce_4B_2C_2H_{2.42}$. The [C−B−B−C] moiety has also been reported in both Nd_2BC and $Ce_6Br_3B_2C_3$, in which the B−B distances were reported to be 1.65(2) and 1.64 Å, while the B−C distances were 1.51(2) and 1.53 Å, respectively.[19,20]

Two interstitial sites are formed by the adjacent layers of cerium ions in the structure: tetrahedral sites and octahedral sites occur in a 2:1 ratio. The single-crystal X-ray data for the title compound indicated an electron density peak in the octahedral site (on a special position 2a Wyckoff site) but none in the tetrahedral site. Since the EDS data supported the presence of fluorine in the material, a fluorine atom was placed on the octahedral interstitial site. The resulting Ce−F distances are 2.7669(2) and 2.9277(4) Å, which are larger than those reported for CeF_3 (2.400(3)−2.621(5) Å).[21] This octahedral interstitial site does decrease in size compared to the hydride analogue $Ce_4B_2C_2H_{2.42}$ (H_{oct}−Ce distances of 2.798 and 2.941 Å),[9] which may explain the slight shrinking of the unit cell. This may be due to the relative hardness of the F^- anion, which is typically reported with ionic radii between 1.33 and 1.36 Å, compared to the softer, more polarizable H^- anion (with a wider range of reported radii, between 1.27 and 1.52 Å), which may expand or contract more easily to fit an interstitial site.[22] The occupancy of the fluorine site was allowed to vary in the SC-XRD data refinement. Several crystals were analyzed, with the fluorine occupancy ranging from 11(3) to 19(3) %. Because of the low occupancy of this site, it led us to question if this could be a mixed site with hydrogen.

To shed light on this, as well as the possible incorporation of hydrides on the tetrahedral interstitial site (as observed for $Ce_4B_2C_2H_{2.42}$), neutron diffraction data were collected in order to take advantage of the distinctive strong negative neutron scattering of hydrogen. The data clearly indicated the presence of hydrogen on both the tetrahedral and octahedral interstitial sites. The tetrahedral site (4i Wyckoff position) was assigned as occupied only by hydrogen and then allowed to refine; the resulting occupancy was 71(2)%. The Ce−H_{tet} distances are 2.417(3), 2.418(4), and 2.425(4) Å. This is slightly larger than the 2.395 Å Ce−H distances found in the tetrahedral site of $CeH_{2.73}$ but is slightly smaller than the Ce−H_{tet} distances in $Ce_4B_2C_2H_{2.42}$, which are 2.437−2.470 Å.[9,23] The partial occupancy of this site is notable, given the fact that this corresponding site in $Ce_4B_2C_2H_{2.42}$ was fully occupied by hydride.

The filling of the octahedral site proved to be more complex. A negative neutron peak was observed at the 2a Wyckoff site in the center of the octahedral site; however, it was unknown how

https://doi.org/10.1021/acs.cgd.3c00512
Cryst. Growth Des. 2023, 23, 5919−5924

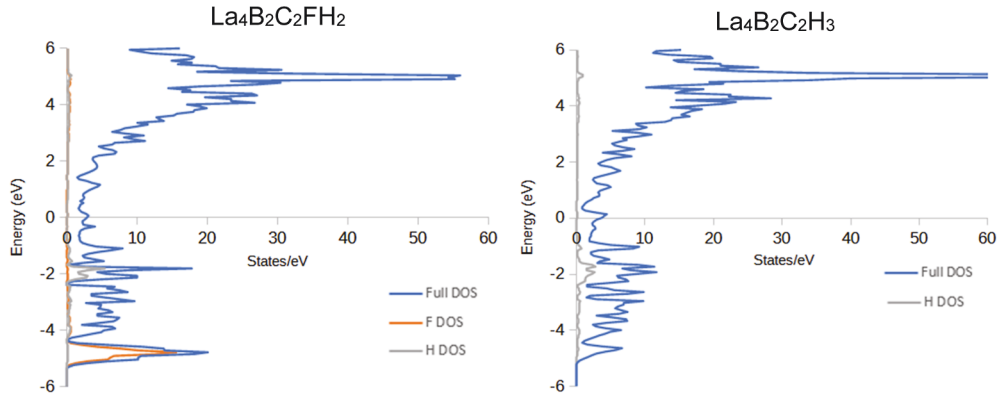

Figure 4. DOS data for two models of $Ce_4B_2C_2F_{0.14}H_{2.26}$. The Fermi level is set to 0 eV.

much of that was due to hydrogen and how much of a positive fluorine peak was contributing to that site. The occupancy of the fluorine was constrained to 13.6% (the average value of fluorine occupancy from multiple SC-XRD datasets), and the occupancy of the hydrogen was allowed to vary, leading to an occupancy of 84(5)%. The combined occupancy of 13.6% fluorine and 84% hydrogen indicates that this mixed site is almost completely filled. The distance between the octahedral mixed site and the adjacent tetrahedral hydride site is 3.21 Å.

Magnetic Measurements. In Figure 3, the temperature-dependent magnetic susceptibility and field-dependent magnetization data are shown for $Ce_4B_2C_2F_{0.14}H_{2.26}$ (red) and compared to our previously reported data for $Ce_4B_2C_2H_{2.42}$ (blue). The temperature dependence data for $Ce_4B_2C_2F_{0.14}H_{2.26}$ was fitted using the extended Curie−Weiss law, $(\chi(T) = C/(T - \Theta) + \chi_0)$, with χ_0 being −0.0137 emu/mol. The effective moment per cerium (μ_{eff}) was calculated to be 2.54 μ_B, and the Weiss constant θ was found to be −166.87 K. This large negative value of θ is to be expected for cerium intermetallics, indicating hybridization between f- and conduction electrons; a similar large value was seen for the hydride analogue.

The susceptibility data for the hydride $Ce_4B_2C_2H_{2.42}$ exhibits a cusp at T_N = 7.7 K that corresponds to a canted antiferromagnetic ordering. With the inclusion of fluorine, the cusp is nearly gone. Introduction of fluorine on the octahedral sites of $Ce_4B_2C_2F_{0.14}H_{2.26}$ modifies the magnetic coupling and hinders long-range ordering. The small feature that does appear at 7.7 K may be due to the regions of the sample that are hydride rich. The canted antiferromagnetism in $Ce_4B_2C_2H_{2.42}$ also caused splitting of the field cooled (FC) and the zero FC measurements below 7.7 K and a slight hysteresis in the magnetization data; both of these behaviors (which are likely related to domain formation of the net ferromagnetic moments caused by canted spins) are gone in the $Ce_4B_2C_2F_{0.14}H_{2.26}$ analogue. The introduction of fluorine into the structure modifies the unit cell size and changes the Ce−Ce distances; it also causes an additional local disorder. Both these factors can disrupt magnetic coupling, leading to paramagnetic behavior.

Electronic Structure Calculations. DOS calculations were carried out by modeling cerium atoms as lanthanum to avoid a partially filled f-shell. Because the octahedral site in $Ce_4B_2C_2F_{0.14}H_{2.26}$ is a mixed H/F site, two models were used to estimate the actual DOS. Those models are $La_4B_2C_2FH_2$ with the octahedral site fully occupied by fluorine (and tetrahedral site fully occupied with hydrogen), and $La_4B_2C_2H_3$ with the octahedral site fully occupied by hydrogen (and tetrahedral site fully occupied with hydrogen). From the DOS plot shown in Figure 4, it can be seen that the fluorine s- and p-orbitals are filled well below the Fermi level at approximately −5 eV. The high negative value for the fluorine states is understandable, considering that fluorine is the most electronegative element and is therefore largely ionic. The filled hydrogen states can also be seen at −2 eV. The empty La f-orbital contributes to the narrow collection of states at 5 eV. La s, p, and d orbitals produce the states at E_F, indicating metallic behavior. The partial occupancy of the hydride sites will cause a lower overall electron count, potentially placing the Fermi level in the pseudogap at around −0.5 eV; this likely stabilizes the compound (see Figure 4).

CONCLUSIONS

$Ce_4B_2C_2F_{0.14}H_{2.26}$ was grown by metal flux synthesis from Ce/Cu flux with the addition of boron, anthracene, and decafluorobiphenyl. The use of a molecular C_xF_y species during flux growth of intermetallics is proven to be a useful way to gently fluorinate products, avoiding the full oxidation to ionic metal fluorides that results using other methods. SCXRD confirmed the presence of fluorine on an octahedral interstitial site. Single-crystal neutron diffraction was used to confirm the presence of hydrogen mixing in the octahedral site as well as partially occupying a tetrahedral interstitial site. The magnetic susceptibility of $Ce_4B_2C_2F_{0.14}H_{2.26}$ shows the disappearance of the magnetic ordering that occurs at 7.7 K for the hydride $Ce_4B_2C_2H_{2.42}$. Mixing of hydrogen and fluorine on interstitial sites may prove to be a useful method for tailoring magnetic properties of intermetallic compounds. This could be carried out either by the use of separate C_xH_y and C_xF_y reactants as was done in this work, or by exploration of $C_xH_yF_z$ compounds as sources of both interstitial atoms. This may lead to new magnetic materials or new superconductors.

ASSOCIATED CONTENT

Supporting Information

The Supporting Information is available free of charge at https://pubs.acs.org/doi/10.1021/acs.cgd.3c00512.

Depiction of the reaction set up used for the synthesis of the title compound (PDF)

Accession Codes

CCDC 2259229−2259230 contain the supplementary crystallographic data for this paper. These data can be obtained free of charge via www.ccdc.cam.ac.uk/data_request/cif, or by

https://doi.org/10.1021/acs.cgd.3c00512
Cryst. Growth Des. 2023, 23, 5919−5924

emailing data_request@ccdc.cam.ac.uk, or by contacting The Cambridge Crystallographic Data Centre, 12 Union Road, Cambridge CB2 1EZ, UK; fax: +44 1223 336033.

AUTHOR INFORMATION

Corresponding Author

Susan E. Latturner − *Department of Chemistry and Biochemistry, Florida State University, Tallahassee, Florida 32306, United Stated;* orcid.org/0000-0002-6146-5333; Email: slatturner@fsu.edu

Authors

James T. Larson − *Department of Chemistry and Biochemistry, Florida State University, Tallahassee, Florida 32306, United Stated*

Christina Hoffmann − *Neutron Scattering Division, Oak Ridge National Laboratory, Oak Ridge, Tennessee 37831, United Stated*

Complete contact information is available at: https://pubs.acs.org/10.1021/acs.cgd.3c00512

Notes

The authors declare no competing financial interest.

ACKNOWLEDGMENTS

This research was supported by the National Science Foundation Division of Materials Research (grants DMR-18-08471 and DMR-21-26077). This work used the X-ray Characterization Center in the Department of Chemistry and Biochemistry at Florida State University (FSU075000XRAY). The Scanning Electron Microscope in the Biological Sciences Imaging Resource (BSIR) of the FSU Department of Biology was also used; we thank Dr. Eric Lochner for assistance with this instrument. Single-crystal neutron diffraction data were collected using the TOPAZ instrument (BL-12) at the Spallation Neutron Source at the Oak Ridge National Laboratory, a DOE Office of Science User Facility.

REFERENCES

(1) Ruderman, M. A.; Kittel, C. Indirect Exchange Coupling of Nuclear Magnetic Moments by Conduction Electrons. *Phys. Rev.* **1954**, *96*, 99−102.

(2) Parkin, S. S. P.; Mauri, D. Spin engineering: Direct determination of the Ruderman-Kittel-Kasuya-Yosida far-field range function in ruthenium. *Phys. Rev. B: Condens. Matter Mater. Phys.* **1991**, *44*, 7131−7134.

(3) Okamoto, H. Supplemental Literature Review of Binary Phase Diagrams: Al-Mg, Bi-Sr, Ce-Cu, Co-Nd, Cu-Nd, Dy-Pb, Fe-Nb, Nd-Pb, Pb-Pr, Pb-Tb, Pd-Sb, and Si-W. *J. Phase Equilib. Diffus.* **2015**, *36*, 183−195.

(4) Okamoto, H. Ce-Ni (Cerium-Nickel). *J. Phase Equilib. Diffus.* **2009**, *30*, 407.

(5) Benbow, E. M.; Dalal, N. S.; Latturner, S. E. Spin Glass Behavior of Isolated, Geometrically Frustrated Tetrahedra of Iron Atoms in the Intermetallic La21Fe8Sn7C12. *J. Am. Chem. Soc.* **2009**, *131*, 3349−3354.

(6) Zhou, S.; Mishra, T.; Lyman, D.; Tucker, P.; Latturner, S. E. New cerium cobalt borocarbide synthesized from eutectic metal flux mixture. *Inorg. Chem. Front.* **2017**, *4*, 450−455.

(7) Tucker, P. C.; Nyffeler, J.; Chen, B.; Ozarowski, A.; Stillwell, R.; Latturner, S. E. A Tale of Two Metals: New Cerium Iron Borocarbide Intermetallics Grown from Rare-Earth/Transition Metal Eutectic Fluxes. *J. Am. Chem. Soc.* **2012**, *134*, 12138−12148.

(8) Engstrand, T. O.; Cope, E. M.; Vasquez, G.; Haddock, J. W.; Hertz, M. B.; Wang, X.; Latturner, S. E. Flux Synthesis of a Metal Carbide Hydride Using Anthracene As a Reactant. *Inorg. Chem.* **2020**, *59*, 11651−11657.

(9) Hertz, M. B.; Baumbach, R.; Wang, X.; Latturner, S. E. Unexpected Hydride: Ce4B2C2H2.42, a Stuffed Variant of the Nd2BC Structure Type. *Cryst. Growth Des.* **2021**, *21*, 5164−5171.

(10) CrysAlisPRO. *Oxford Diffraction*; Agilent Technologies UK Ltd: Yarnton, England, 2014.

(11) Hubschle, C. B.; Sheldrick, G. M.; Dittrich, B. ShelXle: a Qt graphical user interface for SHELXL. *J. Appl. Crystallogr.* **2011**, *44*, 1281−1284.

(12) Zikovsky, J.; Peterson, P. F.; Wang, X. P.; Frost, M.; Hoffmann, C. CrystalPlan: an experiment-planning tool for crystallography. *J. Appl. Crystallogr.* **2011**, *44*, 418−423.

(13) Arnold, O.; Bilheux, J. C.; Borreguero, J. M.; Buts, A.; Campbell, S. I.; Chapon, L.; Doucet, M.; Draper, N.; Ferraz Leal, R.; Gigg, M. A.; et al. Mantid—Data analysis and visualization package for neutron scattering and μ SR experiments. *Nucl. Instrum. Methods Phys. Res., Sect. A* **2014**, *764*, 156−166.

(14) Schultz, A. J.; Jørgensen, M. R. V.; Wang, X.; Mikkelson, R. L.; Mikkelson, D. J.; Lynch, V. E.; Peterson, P. F.; Green, M. L.; Hoffmann, C. M. Integration of neutron time-of-flight single-crystal Bragg peaks in reciprocal space. *J. Appl. Crystallogr.* **2014**, *47*, 915−921.

(15) Tank, R.; Jepsen, O.; Burkhardt, A.; Andersen, O. *The TB-LMTO-ASA Program*, 1994.

(16) Blöchl, P. E.; Jepsen, O.; Andersen, O. K. Improved tetrahedron method for Brillouin-zone integrations. *Phys. Rev. B: Condens. Matter Mater. Phys.* **1994**, *49*, 16223−16233.

(17) Vaney, J.-B.; Vignolle, B.; Demourgues, A.; Gaudin, E.; Durand, E.; Labrugère, C.; Bernardini, F.; Cano, A.; Tencé, S. Topotactic fluorination of intermetallics as an efficient route towards quantum materials. *Nat. Commun.* **2022**, *13*, 1462.

(18) Larson, J. T.; Latturner, S. E. Flux growth of an intermetallic with interstitial fluorides via decomposition of a fluorocarbon. *Inorg. Chem.* **2023**, *62*, 1508−1512.

(19) Mattausch, H.; Oeckler, O.; Simon, A. B and B−C as interstitials in reduced rare earth halides. *Inorg. Chim. Acta* **1999**, *289*, 174−190.

(20) Babizhetskyy, V.; Köhler, J.; Mattausch, H.; Simon, A. Synthesis, structure and properties of Nd2BC containing the trans-dibora−(1,3)-butadiene [C=B−B=C]8−-unit. *Z. Krist.* **2011**, *226*, 93−98.

(21) Cheetham, A. K.; Fender, B. E. F.; Fuess, H.; Wright, A. F. A powder neutron diffraction study of lanthanum and cerium trifluorides. *Acta Crystallogr., Sect. B* **1976**, *32*, 94−97.

(22) Messer, C. E. Hydrides versus fluorides: Structural comparisons. *J. Solid State Chem.* **1970**, *2*, 144−155.

(23) Kost, M. E.; Gol'der, G. A. The Crystal Structure And Density Of Cerium Hydrides. *Zh. Neorg. Khim.* **1959**, *4*, 1488−1490.